A Hydrophobic Photolabel Inhibits Nicotinic Acetylcholine Receptors via Open-Channel Block Following a Slow Step†

Stuart A. Forman*

Department of Anesthesia & Critical Care, Massachusetts General Hospital, Boston, Massachusetts 02114, and Department of Anaesthesia, Harvard Medical School, Boston, Massachusetts 02115

Received June 23, 1999; Revised Manuscript Received August 27, 1999

ABSTRACT: 3-(Trifluoromethyl)-3-(*m*-iodophenyl)diazirine (TID) is a hydrophobic inhibitor of nicotinic acetylcholine receptors (nAChRs) and a photolabel that incorporates both at the lipid−protein interface and within the gated pore. On the basis of *Torpedo* vesicle studies, TID is thought to selectively inhibit the closed nAChR state. The nAChR site(s) mediating TID inhibition is unknown. We investigated the state dependence and kinetics of TID inhibition electrophysiologically using rapidly superfused membrane patches expressing mouse muscle nAChRs. Currents from patches simultaneously exposed to ACh and TID show no inhibition of peak currents relative to acetylcholine (ACh) alone but demonstrate slow (10 s^{-1}) TID inhibition. Patch preexposure to TID before ACh results in a burst of current followed by rapid [TID]-dependent inhibition at a bimolecular rate of 1.8×10^8 M^{-1} s^{-1}, indicating that TID selectively inhibits open channels. We also determined sensitivity to TID in two nAChRs containing mutations in their pore-forming M2 domains. The αL251T mutation eliminates sensitivity to TID inhibition, while the αS252I mutation enhances this sensitivity 4-fold compared to wild type. These results indicate that TID inhibition of nAChRs follows two distinct kinetic steps. The rate-limiting step, which shows features suggesting a diffusion barrier, precedes rapid open-state-dependent TID binding to an inhibition site near the putative nAChR gate.

The nicotinic acetylcholine receptor (nAChR)[1] is a ligand-gated ion channel found in postsynaptic membranes of neuromuscular junctions and electric organs of eels and rays (*1*). Acetylcholine binds to the nAChR, inducing rapid gating of its cation-selective channel, which depolarizes postsynaptic cells. This receptor is the best-characterized member of a superfamily of receptors that also includes $GABA_A$, $5\text{-}HT_3$, glycine, and neuronal nicotinic receptors (*2*). The structure of the receptor has been defined to 4.6 Å by cryoelectron microscopy (*3*), and its important functional domains have been identified. Each of the five homologous subunits ($\alpha_2\beta\gamma\delta$) in a nAChR monomer contains a large amino-terminal cytoplasmic domain and four putative transmembrane domains (M1−M4). Photolabeling, mutagenesis, and cysteine modification studies indicate that the cation-conductive transmembrane pore of nAChR is lined by residues from the five homologous M2 domains, which are thought to form predominantly α-helical structures (*4*−*6*).

3-(Trifluoromethyl)-3-(*m*-iodophenyl)diazirine (TID) is a highly hydrophobic nAChR inhibitor and an informative photoactivable probe of nAChR structure (*7*, *8*). Rapid $^{86}Rb^+$ quenched-efflux studies in nAChR-rich *Torpedo* vesicles show an unusual pattern of inhibition by TID. While simultaneous exposure to both agonist and TID fails to inhibit nAChR function, incubation with TID prior to agonist stimulation potently inhibits $^{86}Rb^+$ efflux without directly inducing desensitization (*8*, *9*). These results imply that TID selectively inhibits the resting nAChR state.

Photoactivated ^{125}I-TID incorporates into resting and desensitized *Torpedo* nAChRs at amino acids located both in the gated transmembrane pore (M2 domains) and at the putative lipid−protein interface formed by the M3 and M4 domains of each subunit. The pattern of ^{125}I-TID labeling in M3 and M4 domains indicates α-helical structures (*10*, *11*). The M2 domains of resting nAChRs are photolabeled by ^{125}I-TID at homologous leucines αL251, βL257, γL260, and δL265 (9′ loci) and about one helical turn toward their cytoplasmic (C-terminal) ends at αV255, βV261, γI264, and δV269 (13′ loci; *4*, *10*, *12*). In agonist-desensitized nAChRs, ^{125}I-TID labeling of M2 is reduced and shifted toward N-terminal residues (*12*). Recently, time-resolved photolabeling of *Torpedo* nAChR with ^{125}I-TID has revealed the rates at which TID binds nAChR (*13*). It is not known which, if any, of the photolabeled domains forms the site where TID inhibits nAChR function.

In this study, we applied rapid-superfusion patch-clamp electrophysiology to better define the state dependence and kinetics of nAChR inhibition by TID. In addition, we tested the hypothesis that TID acts at a site within the transmembrane pore by investigating whether pore mutations affected sensitivity to TID inhibition.

† This research was supported by the MGH Department of Anesthesia & Critical Care and a grant from the National Institutes of General Medical Sciences, P01-GM58448.

* Address correspondence to the author at Department of Anesthesia & Critical Care, CLN-3, Massachusetts General Hospital, Boston, MA 02114. Phone (617) 724-5156; Fax (617) 724-2712; E-mail forman@helix.mgh.harvard.edu.

[1] Abbreviations: ACh, acetylcholine; EGTA, ethylene glycol bis(β-aminoethyl ether)-*N*,*N*,*N*′,*N*′-tetraacetic acid; Hepes, *N*-(2-hydroxyethyl)piperazine-*N*′-2-ethanesulfonic acid; nAChR, nicotinic acetylcholine receptor; PCR, polymerase chain reaction; TID, 3-(trifluoromethyl)-3-(*m*-iodophenyl)diazirine; TLC, thin-layer chromatography.

10.1021/bi9914457 CCC: $18.00
Published on Web 10/14/1999

EXPERIMENTAL PROCEDURES

Materials. 3-(Trifluoromethyl)-3-(*m*-iodophenyl)diazirine (TID; >99% by TLC) was synthesized and generously provided by Dr. Shaukut Hussain (Massachusetts General Hospital, Boston, MA). Stock TID in ethanol was stored in the dark at −80 °C, and dissolved in buffer immediately prior to use. All other chemicals were purchased from Sigma Chemical Co. (St. Louis, MO) and were of reagent grade or better

Site-Directed Mutagenesis. cDNAs for α, *β*, *γ*, and *δ* subunits of the mouse muscle nAChR were a gift from Dr. James McLaughlin (University of South Carolina, Charleston, SC). Mutant cDNAs were constructed by high-fidelity PCR oligonucleotide-directed mutagenesis (*14*). All mutations and transferred sequences were confirmed by dideoxynucleotide sequencing.

Xenopus Oocyte Expression. Methods for oocyte expression were previously described (*15*). After incubation for 48−72 h, oocytes were manually stripped of their vitelline membranes for patch-clamp electrophysiology.

Patch-Clamp Electrophysiology. Rapid patch superfusion experiments were performed at room temperature (20−22 °C). Patch pipets were fire-polished to give open tip resistance of 1.5−3 MΩ. Both inside and outside buffers were K-100 (in millimolar: 97 KCl, 1 $MgCl_2$, 0.2 EGTA, and 5 K−Hepes, pH 7.5). Oocyte membrane patches were excised in the outside-out configuration and held at −50 mV. Currents through the patch-clamp amplifier (Axopatch 200A; Axon Instruments, Foster City, CA) were filtered (8-pole bessel, 1−2 kHz) and digitized at 2−5 kHz by use of a Digidata 1200 series interface and pClamp7.0 software (both from Axon Instruments, Foster City, CA) on a PC.

Rapid Superfusion. Rapid superfusate switching (0.4−1.2 ms, measured with open pipet junction currents) was achieved by use of a dual piezo actuator coupled to a quad (2 by 2) perfusion pipet delivering solutions from four reservoir syringes. High-voltage steps, triggered by computer-controlled signals, drove the two orthogonally coupled piezo bimorph elements. In this way, movements that brought adjacent barrels of the quad pipet into position to superfuse the outside-out patch were achieved. Specific superfusion protocols and the solutions used are described in Results.

Data Analysis. Rapid multichannel current traces displayed in figures are averages of 4−8 recordings from a single patch, except where noted. Values are reported as mean ± standard deviation. Nonlinear least-squares fits were performed with Origin software (Microcal Inc., Northampton, MA).

RESULTS

The kinetics and state dependence of TID inhibition were studied in rapidly superfused excised oocyte membrane patches expressing mouse muscle nAChRs. By use of different superfusion protocols, TID actions on both open and closed channels were compared. Simultaneous application of up to 5 μM TID with saturating ACh (1 mM) activation of mouse nAChRs resulted in negligible inhibition of peak currents when compared to control currents with ACh alone (Figure 1, panels A and B). However, the rate of current decay in the presence of 5 μM TID (average rate = 16 ± 5 s^{-1}; $n = 5$) appeared about 2-fold faster than the rate of mouse nAChR desensitization induced by high ACh

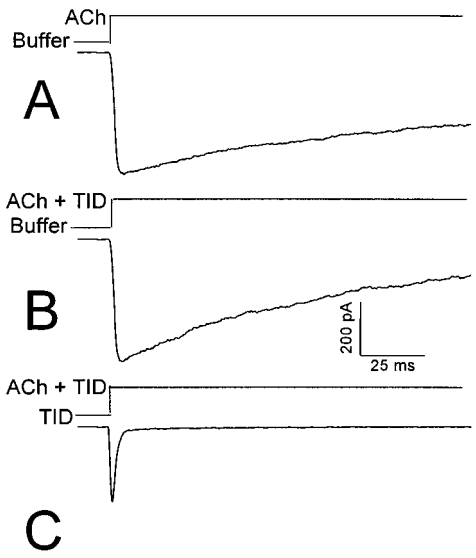

FIGURE 1: Inhibition of mouse nAChR requires prolonged exposure to TID. Three current traces from the same outside-out patch expressing wild-type mouse muscle nAChRs were elicited with different TID/ACh superfusion protocols. Superfusate solutions are labeled above each trace. Panel A shows a control current elicited with 1 mM ACh alone, demonstrating rapid current activation followed by desensitization. Fitting to a single-exponential function revealed a desensitization rate of 6 ± 1 s^{-1}. Panel B was recorded with simultaneous application of 5 μM TID and 1 mM ACh. The trace differs from control only in the apparent rate of current decay, which is 13 ± 1 s^{-1}. Panel C: After preexposure of the patch to TID for over 1 min, application of 1 mM ACh plus 5 μM TID elicited a brief current burst followed by rapid current decay at a rate of 680 ± 40 s^{-1}.

alone (average rate = 8 ± 2 s^{-1}; $n = 5$). Thus, after hundreds of milliseconds, ACh-elicited current in the presence of TID fell below control levels. In the presence of 5 μM TID, the total current passed during a 200 ms ACh pulse was reduced by 43 ± 5% ($n = 5$).

When patches expressing nAChRs were exposed to 5 μM TID for several minutes before ACh activation, much more inhibition of currents was observed (Figure 1C). The 200 ms integrated current was reduced 98.5 ± 0.6% ($n = 5$) by 5 μM TID. Of note, nAChRs activated by ACh after preincubation with TID consistently produced a burst of current that accounted for almost all of the residual current. In the data shown in Figure 1C, the peak current (I_{peak}) after TID preincubation was 60% of control I_{peak}. This current decayed within a few milliseconds to a much smaller steady-state current.

To more readily observe the rate of onset of TID inhibition when coapplied with ACh, patches expressing nAChR were activated with a low ACh concentration (5 μM ≈ EC_{10}) that caused slower desensitization. When TID was simultaneously applied with 5 μM ACh, current decay (Figure 2, note change in time scale from Figure 1) displayed two apparent rate components. The faster component, accounting for most of the decay, was characterized by rates that increased nonlinearly with TID up to 50 μM (range 5−17 s^{-1} with gravity-driven superfusion, 8−32 s^{-1} at 10 times gravity superfusion rate). The smaller, slower component of current decay paralleled desensitization at 5 μM ACh. The apparent rate of TID inhibition (fast component) varied less than 2-fold when the superfusion rate of the ACh/TID solution was increased up to 13-fold by pressurizing the reservoir syringe.

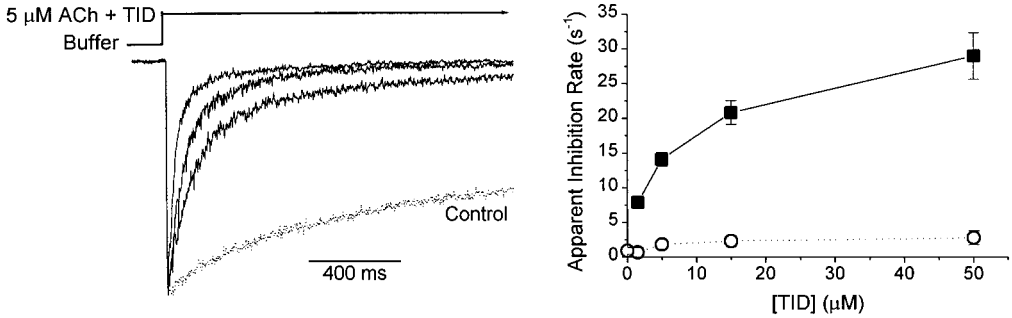

FIGURE 2: Activation with low ACh reveals slow TID inhibition rate. (Left) TID inhibition of mouse nAChRs was observed in patch currents stimulated with low ACh (5 μM $\approx$ EC_{10}) that induced very slow desensitization (dotted trace). Solutions containing ACh + TID (0, 1.5, 15, and 50 μM TID concentrations shown) were superfused from a pressurized syringe at 10 times the gravity-driven flow. Traces were fit to double exponential functions. (Right) Fast (■) and slow (○) decay rate constants (average ± SD, $n = 4$) are plotted.

The rate of recovery from TID inhibition was also measured in patches activated with 5 μM ACh. After 500 ms of exposure to 5 μM TID, current recovered with a time constant of 2−3 s (data not shown). Up to 15% of the ACh-elicited current was irreversibly inhibited by TID or recovered very slowly (time constant > 30 s).

The rate of TID action on resting nAChRs was measured with a three-solution sequential superfusion protocol delivered via a dual axis piezo-driven quad pipet. After variable periods (50−1400 ms) of preexposure to TID, currents were activated with 1.0 mM ACh plus TID for 100 ms and then recovered in buffer for 20 s before the next sweep (Figure 3A). These experiments revealed the multistep nature of TID interactions with nAChR (Figure 3B). ACh-stimulated I_{peak} diminished with TID preexposure, revealing at least two exponential rates. The faster component of peak current reduction was characterized by rates ranging from 5 to 15 s^{-1}, while the slower component showed rates of 1−2 s^{-1}. The extent of both components increased at higher TID concentrations. With intersweep periods of 20 s, recovery of peak ACh response after 10 sweeps was usually incomplete. Washout periods of up to 2 min did not significantly alter the degree of irreversible current loss, so it was not experimentally practical to further investigate this process.

Peak current reduction in the presence of TID was paralleled by the development of increasingly rapid inhibition after ACh activation. For example, in sweep 1 of Figure 3B a cumulative TID exposure time of 150 ms (50 ms preincubation and 100 ms with ACh) is associated with 42% inhibition, which develops during the 100 ms ACh pulse. After TID preexposures longer than 1 s (sweeps 8−10 of Figure 3B), inhibition after ACh activation develops within 10 ms and is more profound (68% reduction relative to I_{peak}). To estimate the rate at which rapid TID inhibition developed in the resting state, we normalized the TID-inhibited "steady-state" current (I_{ss}) to I_{peak} in each sweep and plotted this ratio against cumulative TID exposure time (Figure 3C). The rates at which I_{ss}/I_{peak} declined in this experiment varied from 4 to 16 s^{-1} but showed no consistent dependence on TID concentration (Figure 3D).

After preincubation with TID, both the rate and extent of the rapid inhibition seen after ACh application strongly depended on TID concentration (Figure 4). As TID increased, the rate of current inhibition grew, maintaining a linear relationship with a slope of 1.8×10^8 M^{-1} s^{-1} (Figure 4). While the fastest rates of inhibition ($\sim$ 1200 s^{-1}) were nearly limited by data sampling frequency (2 kHz), there was no

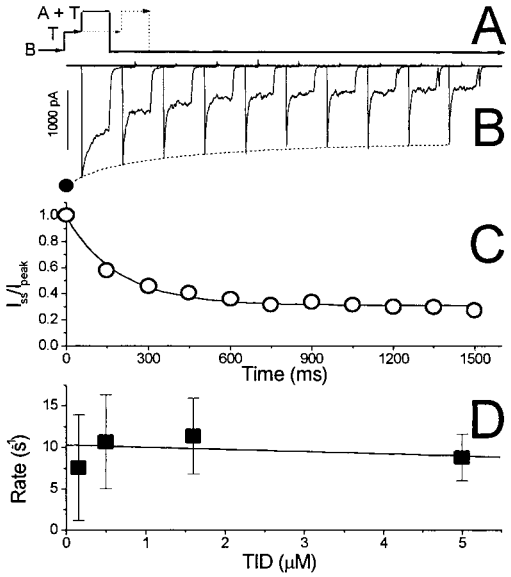

FIGURE 3: The slow step is followed by rapid TID inhibition after channel activation. (A) Outside-out oocyte patches were subjected to a three-solution superfusate protocol as diagrammed. After a control 100 ms pulse in ACh alone (1.0 mM; peak current represented by the ●), the patch was subjected to increasing periods of TID (T) superfusion [t (ms) = 50 + 150(i − 1), i = 1−10], followed by a 100 ms period in ACh plus TID (A + T). The patch was then superfused with buffer alone (B) during the remainder of each 2 s sweep and remained in buffer for 20 s before the next sweep. For clarity, only the first two sweeps are diagrammed and the protocol for sweep 1 is highlighted. The time base is the same as for panels B and C. (B) Individual traces from a patch expressing mouse nAChRs exposed for variable periods to 0.5 μM TID and activated with 1.0 mM ACh plus TID. Peak ACh-activated currents (I_{peak}) diminished with TID preincubation and were fitted with a double-exponential function (dashed line). Fitted rates (and fraction inhibition) were 11 ± 9 s^{-1} (0.1 ± 0.1) and 2.0 ± 1.2 s^{-1} (0.26 ± 0.08). Within milliseconds after ACh activation, rapid inhibition is apparent, resulting in a lower steady-state current (I_{ss}). (C) I_{ss} was measured near the end of each ACh application in each sweep from panel B and normalized to the I_{peak} in that sweep. Data were fitted to a single-exponential function (solid line): Fraction inhibition = 0.68 ± 0.01, rate = 5.3 ± 0.2 s^{-1}. (D) The faster of the two fitted rates from experiments similar to those in panel B were averaged ($n \geq 4$ at each TID concentration). The data show no consistent relationship to TID concentration and the linear fit has a slope that is not significantly different from 0 (−69 ± 330 M^{-1} s^{-1}).

flattening of the concentration−rate relationship at up to 5 μM TID. The TID concentration dependence of average I_{ss}/I_{peak} values revealed an IC_{50} of about 100 nM for wild-type mouse nAChRs with a Hill coefficient near 1.0 (Figure 5).

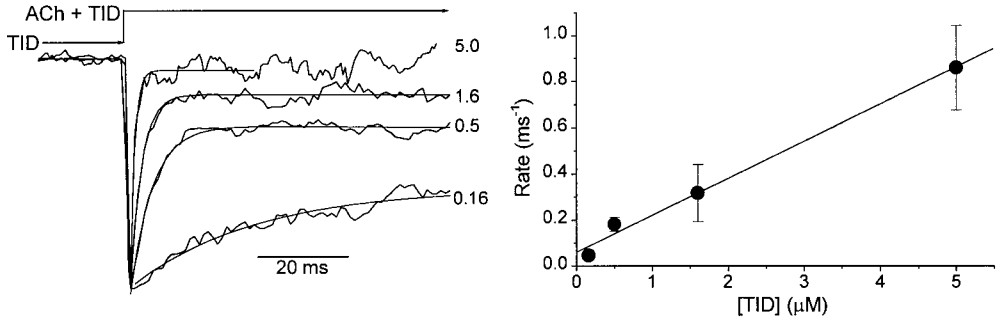

FIGURE 4: Rates of rapid TID inhibition after channel activation. Individual sweeps from experiments such as those in Figure 3B (with TID preincubation ≥ 1.0 s) were selected and the rates and extents of inhibition after ACh activation were determined from single-exponential fits. (Left) Four current traces from separate patches exposed to different TID concentrations are shown, normalized and aligned so that their rising phases overlap. The rates (and fractions) of inhibition by TID are as follows: 0.16 μM, 37 ± 3 s^{-1} (0.41 ± 0.01); 0.5 μM, 210 ± 12 s^{-1} (0.72 ± 0.02); 1.6 μM, 410 ± 30 s^{-1} (0.84 ± 0.02); 5 μM, 1030 ± 70 s^{-1} (0.95 ± 0.03). (Right) Average rapid inhibition rates ($n \geq 4$) are plotted against TID concentration. Linear least-squares gives a slope of (1.8 ± 0.1) × 10^8 M^{-1} s^{-1} and an intercept of 60 ± 30 s^{-1}.

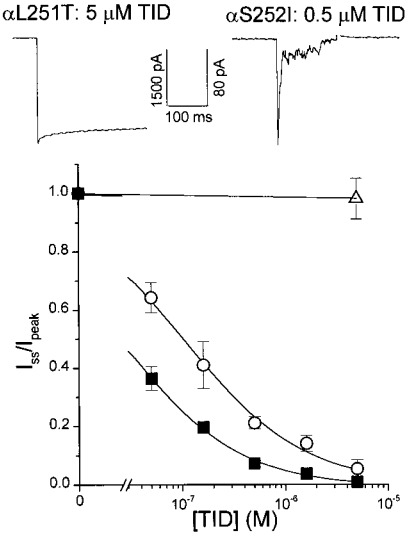

FIGURE 5: Channel mutations alter nAChR sensitivity to TID inhibition. After preincubation with TID for 1 s, currents were recorded from outside out patches expressing mutant channels in the presence of ACh (at least 10 times EC_{50}) and TID (as labeled). (Top) Traces from two different patches expressing either αS252I or αL251T mutant nAChRs in the presence of TID. (Bottom) Steady-state current after rapid inhibition was normalized to peak current and averaged (±SD, $n \geq 4$). Lines through wild-type and αS252I mutant data represent nonlinear least-squares fits with logistic equations of the form $F = 1 - [TID]^n/(IC_{50}{}^n + [TID]^n)$. Fitted IC_{50}s and Hill coefficients (n) are as follows: wild type (○), 102 ± 7 nM (0.8 ± 0.1); αS252I (■), 24 ± 3 nM (0.8 ± 0.1). The αL251T mutant nAChR (△) was insensitive to the highest TID concentration tested (5 μM).

The current burst pattern seen after preequilibration with TID indicated that TID inhibition is dependent on channel gating and therefore likely to be associated with pore structures. We investigated whether hydrophobic mutations at sites near mouse homologues of the TID-photolabeled M2 sites affected nAChR sensitivity to TID. Such mutations have previously been shown to affect nAChR sensitivity to other hydrophobic inhibitors (*14*, *15*). Indeed, α-M2 domain mutations dramatically affected the apparent sensitivity to TID inhibition (Figure 5). At a residue homologous to the labeled 9′ leucines, the mouse αL251T mutation eliminated inhibition by TID. Peak current reduction after preincubation with 5 μM TID for up to 10 s was less than 10%, and rapid inhibition after subsequent ACh activation was under 5%. At an adjacent residue, the αS252I mutation significantly potentiated nAChR inhibition by TID, as illustrated by the reduced I_{ss}/I_{peak} ratios seen in ACh-activated currents (Figure 5, top; compare with wild-type traces in Figure 4). The TID IC_{50} for the αS252I mutation was reduced 4-fold from that for wild type (Figure 5).

DISCUSSION

TID Inhibition Is a Two-Step Process. In rapid quenched $^{86}Rb^+$ flux experiments using nAChR-rich *Torpedo* vesicles, simultaneous application of TID with ACh led to negligible inhibition, while preincubation with TID led to potent inhibition (*9*). In this study, using electrophysiologic monitoring of rapidly superfused oocyte patches expressing mouse nAChRs, simultaneous application of TID with ACh resulted in only modest inhibition, while preincubation with TID resulted in profound inhibition of total current (Figure 1). Thus, when integrated currents are considered, TID effects on nAChRs expressed in oocyte patches closely reflect those observed in *Torpedo* vesicles.

On the basis of the *Torpedo* vesicle experiments, TID was proposed to selectively inhibit the nAChR resting state. However, continuous electrophysiologic recording reveals that a short burst of ACh-activated current flows after preincubation with TID. This brief current burst is inconsistent with the exclusive inhibition of resting receptors, which is predicted to diminish peak currents but not affect the closure or desensitization of open channels. Paradoxically, the rapid electrophysiologic data indicate that TID is a selective inhibitor of the open nAChR state. Why quenched-flux $^{86}Rb^+$ flux experiments in *Torpedo* vesicles failed to detect inhibition by TID during simultaneous application of TID with ACh is explained by comparing panels A and B in Figure 1. With addition of TID, there is negligible inhibition of I_{peak} and very little additional current decay during the initial 7 ms, the period of flux integration used by Wu et al. (*9*). Furthermore, in the *Torpedo* experiments, limited time resolution and lack of continuous ion flux monitoring prevented observation of the early current burst after TID preincubation. Thus, there is little doubt that the state dependence of TID inhibition in *Torpedo* nAChR is the same as that in mouse muscle receptors.

Another apparent discrepancy between our results and the vesicle flux experiments is the apparent inhibitory potency of TID. We estimate an IC_{50} near 100 nM for TID at mouse

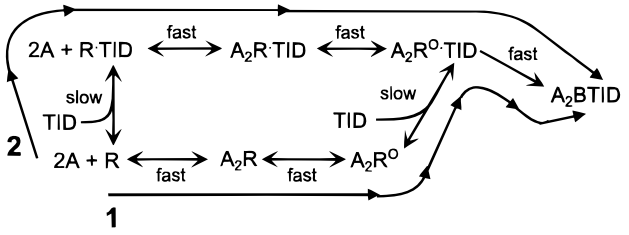

FIGURE 6: Scheme depicting the two-step mechanism leading to TID inhibition. Two pathways from the resting nAChR state (R) to the TID-blocked state (A_2BTID) are shown. In path 1, agonist and TID are presented simultaneously. Agonist rapidly binds and receptors enter the open state (A_2R^o). TID associates slowly with this state and then rapidly blocks once associated. In path 2, TID is present before agonist. TID binds slowly to resting receptors, forming the functionally intact R·TID complex, which then binds agonist (A). A TID-associated open state (A_2R^o·TID) conducts current, which is then rapidly blocked by TID.

nAChRs, while *Torpedo* vesicle flux experiments gave IC_{50}s of 0.4−1 μM (*9*, *12*). Part of this discrepancy may be due to the weighting of integrated flux measurements toward the very early tracer flow, which is weakly inhibited by TID. Moreover, TID is extremely hydrophobic, with an estimated membrane/buffer partition coefficient of 1.5×10^5 (*16*), so that the free aqueous TID concentration after mixing with even small volumes of lipid vesicles may be significantly depleted. In typical native *Torpedo* vesicle flux experiments using 0.1 mg/mL protein with a lipid:protein ratio of 0.5 (*17*), lipid is present at 0.05 mg/mL, which at equilibrium will contain 88% of the TID, an 8-fold depletion of the aqueous concentration. If we correct the IC_{50} measured in *Torpedo* vesicles for TID depletion, the apparent discrepancy in sensitivities vanishes.

When the effects of simultaneous TID/ACh application are considered together with the effects of sequential drug application, they indicate that TID inhibition of nAChRs involves two distinct kinetic steps. A slow step leading to weak TID inhibition precedes rapid TID movement associated with potent inhibition of ACh-activated channels. This slow step represents the rate-limiting step in TID inhibition in both the presence and absence of ACh. A general scheme showing the proposed mechanism of TID inhibition is shown in Figure 6.

Inhibition by TID Follows Rapid Binding to a Site in the Pore. A number of pieces of evidence converge toward a model where TID ultimately inhibits nAChR by binding at a site within the gated pore. Photolabeling in resting and desensitized nAChRs demonstrates that TID reaches the pore-forming M2 domains in the resting state but that labeling of specific side chains changes with the agonist-induced state changes (*12*). Our electrophysiologic study, utilizing rapid solution exchange and continuous current recording, complements and extends the binding data by demonstrating both that TID "waits" until after channel activation to fully inhibit nAChRs and that mutations at loci where TID is thought to interact with the pore radically alter sensitivity to TID inhibition.

The observation of open-state selective inhibition by TID indicates that regions of the pore accessed by TID in the resting state may not form the ultimate site of inhibition. After channel opening, TID rapidly moves into the pore to its ultimate inhibition site. Since open-state TID inhibition rates correlate linearly with concentration (Figure 4), many interchangeable TID molecules must be poised to inhibit the nAChR upon gating. These TID molecules are likely to reside in the water inside the vestibule of the pore, since the outer portion of the pore is photolabeled in the resting state.

Where precisely is the TID inhibition site? The loss of sensitivity to TID with the αL251T mutation suggests that the photolabeled "ring" of leucines at the 9′ level in M2 domains, which has been proposed to form the gating structure within the pore (*3*, *18*), forms the TID inhibition site. It is unlikely that the αL251T mutation simply prevents access to a deeper site, because hydrophobic TID should be able to reach a site on the far side of the gate by passing through the membrane bilayer and entering the pore from the cytoplasmic end.

Although photolabeling shows that TID can reach 9′ leucines in resting state nAChRs, data presented in this study indicate that inhibition of the resting state is very weak. Models where either the gating conformation change induces stronger TID binding or a single TID molecule moves from one pore site to another after channel gating predict open-state inhibition rates that are independent of TID concentration. These are clearly incompatible with the linear concentration−rate relationship for open-channel inhibition (Figure 4). If we accept that TID binds to the outer pore in resting-state nAChRs, then we must postulate that gating enables a second TID molecule to reach the high-affinity open-state site, resulting in inhibition.

The Rate-Limiting Step Is State-Independent. When TID is simultaneously applied with either high or low ACh concentrations (Figures 1 and 2), peak currents are unaffected, and inhibition of current develops over a period of hundreds of milliseconds. Similarly, in experiments where resting-state nAChRs were sequentially exposed to TID for variable durations followed by ACh application (Figure 3), reduction of peak ACh-activated currents and development of subsequent rapid inhibition was seen only after TID exposure for hundreds of milliseconds.

The rate of the slow TID association step is most easily observed when ACh is absent or is present at low concentrations, i.e., when desensitization is slow (Figures 2 and 3). However, these conditions are not equivalent. With sequential superfusion, TID is applied to only resting channels prior to ACh activation and the apparent rate of TID inhibition (about 10 s^{-1}) is demonstrably independent of concentration (Figure 3D). With low ACh stimulation, where a mixture of resting and open channels is present, the apparent rate of inhibition was weakly TID-dependent, ranging from about 8 to about 30 s^{-1} over a 30-fold TID concentration range. While the inhibition rates at TID concentrations below 5 μM are comparable to those derived from sequential superfusion experiments, the higher rates seen at up to 50 μM TID (Figure 2) may reflect the faster delivery of TID used in this experiment. Notably, the rate at which 5 μM TID acted on closed nAChRs (10 s^{-1}) is near the rate at which 5 μM TID inhibits *Torpedo* vesicle flux (*9*).

The rate of the slow step in open-state receptors, measured at high ACh, cannot be directly determined, because agonist-induced desensitization at 1 mM ACh proceeds at a rate close to that of TID inhibition (Figure 1). However, data in Figure 1 suggests that TID acts on open-state nAChRs at about 10 s^{-1}. Maximal ACh-induced desensitization occurs at about 6 s^{-1}, while in the presence of TID, current decays at 13

s^{-1}. Furthermore, the recovery rate from desensitization is slow (3 s^{-1}; *19*) and the recovery rate from TID inhibition is very slow (about 0.5 s^{-1}). If we assume that TID has no effect on agonist-induced desensitization rate (as indicated by our data at low ACh), then the apparent current decay rate should be approximately the sum of the inhibition and desensitization rates. Thus, the rate of TID inhibition in open-state nAChRs is about 7 s^{-1}, close to that established in the closed state.

The observation that TID incubation modestly reduces peak ACh-activated currents (see Figure 3B) indicates that the slow step leads to weak inhibition of resting nAChRs. However, we cannot rule out the possibility that the slow step is functionally silent. In patches where ACh activation is limited by superfusate exchange, I_{peak} may be truncated by the overlap of slow activation and rapid TID inhibition. In addition, the partially irreversible loss of I_{peak} (from long-lived blocked or desensitized nAChRs) may be due to accumulation of inactive nAChRs with repetitive patch activation after exposure to TID.

The lack of TID dependence for the rate-limiting step suggests that it is either a diffusion barrier or a conformational change that TID induces in nAChR that is required for subsequent rapid inhibition of the open state. One possibility we considered is that this step represents partitioning of TID into lipids surrounding nAChR, which act as a buffering phase. If lipid uptake limits the growth of the aqueous TID concentration, then apparent inhibition rates should depend directly on the delivery rate of TID in superfusate. Only a weak dependence on TID superfusion rate was observed, suggesting that lipid uptake alone does not limit the onset of TID inhibition. Another possibility is that the TID pathway to its site is via lipids and that entry into lipids is slow. In stopped-flow experiments, TID (10 μM) quenches vesicle-bound diphenylhexatriene (DPH) fluorescence at rates over 300 s^{-1} (K. W. Miller, personal communication). Thus, TID enters lipids much faster than it inhibits nAChR in either patch perfusion or *Torpedo* vesicle experiments. Further experiments will be required to more fully characterize the slow TID step.

Correlation with Time-Resolved Photolabeling Experiments. In rapid room-temperature *Torpedo* nAChR photolabeling experiments, TID photoincorporation into resting nAChRs is about 50% complete within a few milliseconds, indicating that TID can reach part of the nAChR very rapidly (*13*). The remainder of nAChR photolabeling evolves at a rate near 10 s^{-1}, which corresponds with the rate-limiting step in inhibition. Analysis of nAChR digest fragments in this type of experiment has recently shown that TID sites on M4 domains, at the putative lipid−protein interface, are labeled within a few milliseconds, while subunit fragments containing M2 domains are labeled slowly (K. W. Miller, J. B. Cohen, and D. Chiara, personal communication). These data confirm a mechanism where the slow step in TID inhibition is associated with TID reaching the pore-lining region of nAChR.

ACKNOWLEDGMENT

I thank Dr. Shaukut Hussain for his gift of TID, Carol Gelb for expert technical assistance, and Drs. Keith Miller and Jonathan Cohen for their comments and suggestions.

REFERENCES

1. Changeux, J. P., and Edelstein, S. J. (1998) *Neuron 21*, 959−980.
2. Stroud, R. M., McCarthy, M. P., and Shuster, M. (1990) *Biochemistry 29*, 11009−11023.
3. Miyazawa, A., Fujiyoshi, Y., Stowell, M., and Unwin, N. (1999) *J. Mol. Biol. 288*, 765−786.
4. Blanton, M. P., Dangott, L. J., Raja, S. K., Lala, A. K., and Cohen, J. B. (1998) *J. Biol. Chem. 273*, 8659−8668.
5. Charnet, P., Labarca, C., Leonard, R. J., Vogelaar, N. J., Czyzyk, L., Gouin, A., Davidson, N., and Lester, H. A. (1990) *Neuron 4*, 87−95.
6. Karlin, A., and Akabas, M. H. (1995) *Neuron 15*, 1231−1244.
7. Brunner, J., and Semenza, G. (1981) *Biochemistry 20*, 7174−7182.
8. White, B. H., Howard, S., Cohen, S. G., and Cohen, J. B. (1991) *J. Biol. Chem. 266*, 21595−21607.
9. Wu, G., Raines, D. E., and Miller, K. W. (1994) *Biochemistry 33*, 15375−15381.
10. Blanton, M. P., and Cohen, J. B. (1992) *Biochemistry 31*, 3738−3750.
11. Blanton, M. P., and Cohen, J. B. (1994) *Biochemistry 33*, 2859−2872.
12. White, B. H., and Cohen, J. B. (1992) *J. Biol. Chem. 267*, 15770−15783.
13. Addona, G. H., Kloczewiak, M. A., and Miller, K. W. (1999) *Anal. Biochem. 267*, 135−140.
14. Forman, S. A. (1997) *Biophys. J. 72*, 2170−2179.
15. Forman, S. A., Miller, K. W., and Yellen, G. (1995) *Mol. Pharmacol. 48*, 574−581.
16. White, B. H., and Cohen, J. B. (1988) *Biochemistry 27*, 8741−8751.
17. Sobel, A., Weber, M., and Changeux, J. P. (1977) *Eur. J. Biochem. 80*, 215−224.
18. Unwin, N. (1995) *Nature 373*, 37−43.
19. Dilger, J. P., and Liu, Y. (1992) *Pfluegers Arch. 420*, 479−485.

BI9914457